Observations of Low-Level Baroclinity Generated by Anvil Shadows

PAUL M. MARKOWSKI

School of Meteorology, University of Oklahoma, Norman, Oklahoma

ERIK N. RASMUSSEN

Cooperative Institute for Mesoscale Meteorological Studies, National Severe Storms Laboratory, Boulder, Colorado

JERRY M. STRAKA AND DAVID C. DOWELL

School of Meteorology, University of Oklahoma, Norman, Oklahoma

(Manuscript received 21 May 1997, in final form 9 December 1997)

ABSTRACT

Low-level cooling beneath the cirrus anvil canopies of supercell thunderstorms is documented in two Verification of the Origins of Rotation in Tornadoes Experiment cases and in the 17 May 1981 Arcadia, Oklahoma, supercell. Surface temperature decreases of 3°C or more occurred beneath the anvils within 45 min of the onset of overcast conditions. Cooling was confined to the lowest few hundred meters of the boundary layer, and believed to be due mainly to a deficit in the energy budget following a reduction of incoming shortwave radiation. In the three cases studied, the vertical wind shear was strong; thus, mixing prevented the formation of an inversion layer.

Strong insolation at the ground outside of the anvil shadows coupled with the cooling beneath the cirrus canopies led to corridors of baroclinity along the shadow edges. It is shown that residence times in these baroclinic zones may be long enough for parcels to acquire considerable horizontal vorticity (e.g., $\sim 10^{-2}$ s^{-1}) en route to a storm updraft. Enhancement of the horizontal vorticity of parcels ingested by an updraft may have implications for the dynamics of storm rotation.

1. Introduction

Despite extensive research into severe storm environments during the past 30 years, to our knowledge there has been no formal documentation of possible effects on supercell dynamics due to cirrus anvils. In a past study by Gray and Jacobson (1977), the effect of opaque high cloud cover on the diurnal variation of tropical cumulus convection was studied. The authors considered radiation differences between the cloudy regions and clear-air regions. Moreover, Segal et al. (1986) investigated circulations associated with cloudy–clear air boundaries, but the clouds studied were low clouds (stratus).

Chin (1994) modeled the role of shortwave and longwave radiation on the dynamic and microphysical structure of a convective system. Also discussed were the optical properties of anvils. In his simulation, Chin found that the albedo of the ice anvil ranged from 0.4 to 0.6, while its optical depth, τ, was approximately 4.4. Moreover, roughly a 400 W m^{-2} incoming shortwave radiation difference between the clear air and the region beneath the anvil was modeled. Similar observational findings are presented in this manuscript; however, we observed *net* surface cooling beneath the anvil. In the modeling work of Chin, net cooling was not observed, mainly because of fixed surface conditions. Perhaps of greatest significance, Chin recognized that the impact of the ice phase on the transmission by anvils can influence the surface radiation budget, and could even ''have a significant effect on the large-scale climate.''

Our purpose is to document temperature gradients that have been detected along the edges of anvil shadows. We present three cases in which shading by anvils during the daytime led to differential heating and, ultimately, to the generation of low-level baroclinity (hereafter, ''anvil-generated'' baroclinity). We will show that these baroclinic zones may have been capable of producing a nontrivial amount of horizontal vorticity (e.g., up to 10^{-2} s^{-1}). Horizontal vorticity is converted to vertical vorticity via tilting, then amplified by stretching (e.g., Davies-Jones 1984; Rotunno and Klemp 1985; Klemp 1987). Vertical vorticity (correlated with vertical

Corresponding author address: Paul Markowski, School of Meteorology, University of Oklahoma, 100 E. Boyd Street, Room 1310, Norman, OK 73019.
E-mail: marko@rossby.ou.edu

velocity) is the defining characteristic of supercell storms; thus, means of enhancing low-level horizontal vorticity may have important implications for the dynamics of such storms. Our purpose is *not* to present a new tornadogenesis mechanism. The tornadogenesis issue is beyond the scope of this manuscript.

Horizontal vorticity is generated by buoyancy gradients alone in the Boussinesq approximation (e.g., Klemp and Rotunno 1983; Rotunno et al. 1988). From the two-dimensional horizontal vorticity equation for inviscid Boussinesq flow,

$$\frac{d\eta}{dt} = -\frac{\partial B}{\partial n}, \tag{1}$$

where n is the horizontal distance normal to the baroclinic zone (positive n toward the colder air). In precipitation-free regions, buoyancy, B, can be adequately approximated as

$$B = g\left[\frac{\theta'}{\overline{\theta}} + 0.61(q_v - \overline{q_v})\right], \tag{2}$$

where g is gravitational acceleration, θ is potential temperature, and q_v is the water vapor mixing ratio. Primes and overbars denote perturbations and mean values, respectively. The horizontal vorticity, η, which points along the baroclinic zone (cold air to the right), is

$$\eta = \frac{\partial u}{\partial z} - \frac{\partial w}{\partial n}, \tag{3}$$

where u and w are the horizontal wind component normal to the boundary and the vertical wind component, respectively.

The buoyancy gradients of interest in this paper arose from differential heating due to anvil shadows. Following the onset of overcast conditions beneath a thick cirrus canopy, the amount of shortwave radiation reaching the surface was significantly reduced. This reduction led to net cooling at the surface in the cases studied. Making exact calculations of the amount of expected cooling due to incoming shortwave radiation reduction is outside the scope of the present paper, since measurements of both the upwelling (from the ground) and downwelling (from the anvil) longwave radiation would be required, as well as information about the sensible, latent, and ground heat fluxes, all of which are coupled with the incoming solar shortwave radiation. (It would seem plausible that melting and evaporation of hydrometeors falling from the anvil could cause additional cooling, generally spreading downward, in the direction opposite the radiative cooling.) The cooling occurring within the shadow of the anvil, coupled with insolation outside the shadow, caused a temperature gradient to form.

The intensity of the temperature gradient is a function of the amount of cooling within the anvil shadow and the amount of insolation in the sunlit region outside of the anvil shadow. In theory, this temperature gradient could extend in a full circuit around the anvil shadow. However, we are especially interested in the temperature gradient that inflow parcels encounter en route to the updraft, since these parcels acquire horizontal vorticity via baroclinic generation [according to (1), vorticity generation occurs throughout the layer containing the temperature gradient, the depth of which we have only been able to estimate]. For a typical supercell that is moving eastward and ingesting low-level southeasterly inflow, horizontal vorticity in the inflow is generated in the baroclinic zone along the right side of the anvil shadow, with respect to the storm motion.

The additional amount of horizontal vorticity (which augments the horizontal vorticity present on the larger scale due to the mean vertical shear) acquired by an inflow parcel depends on the strength of the temperature gradient (actually, the virtual potential temperature gradient) as well as the residence time of the parcel in the baroclinic region [from (1); Fig. 1]. Horizontal vorticity generated with a streamwise component will serve to enhance the storm-relative environmental helicity (SREH; Davies-Jones 1984; Lilly 1986) already present due to the low-level vertical shear. SREH has been shown to be the source for net updraft rotation in supercells.[1] Thus, the observations we present of anvil-generated baroclinity may have implications for the origin or enhancement of updraft rotation in thunderstorms. [Hereafter, we choose to replace SREH with SRH (storm-relative helicity), since it is difficult to define exactly what constitutes ''environmental helicity,'' especially after the horizontal vorticity present on the larger scale has been augmented by baroclinic generation in small-scale regions.]

In section 2, we present the pertinent observations. In section 3, we show that the effectiveness of anvil-generated baroclinity in developing horizontal vorticity should be related to hodograph structure. Some final remarks are provided in section 4.

2. Cases

In this section we present findings from three cases. The first two were operations days during the Verification of the Origins of Rotation in Tornadoes Exper-

[1] Enhancements of crosswise vorticity also may be of importance in mesocyclogenesis and tornadogenesis. Tilting and stretching of crosswise vorticity produces vertical vorticity (Davies-Jones 1984; Rotunno and Klemp 1985), just no *net* updraft rotation (a pair of counterrotating vortices occupies the updraft instead, either one of which, or both, could still go on to produce a tornado). The relationship between streamwise vorticity and tornadoes may be largely associative, since parcel trajectories through baroclinic zones that allow for the longest residence times and baroclinic horizontal vorticity generation (i.e., trajectories that cross through baroclinic zones at small angles, nearly parallel to buoyancy isopleths) inherently have a large streamwise component.

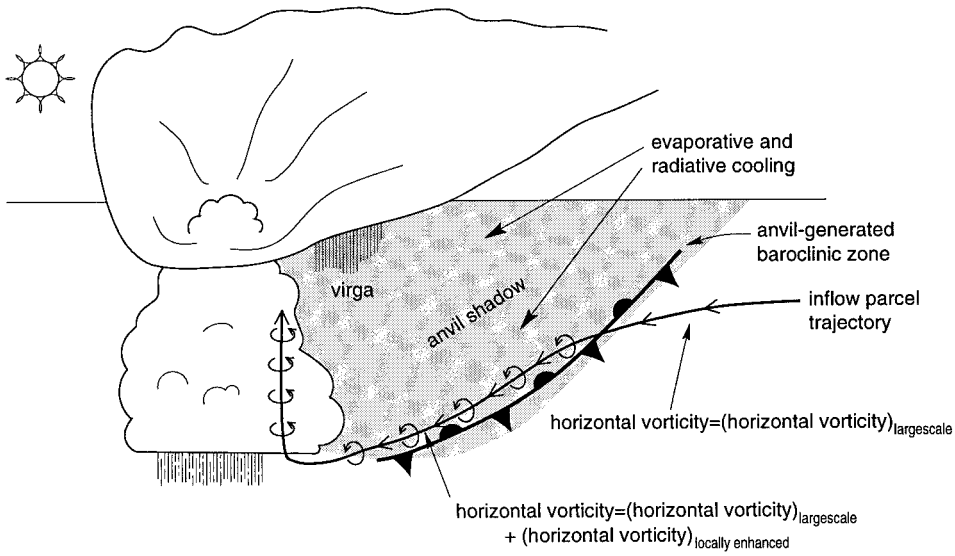

FIG. 1. A conceptual model for the enhancement of low-level horizontal vorticity by an anvil-generated baroclinic zone. The amount of horizontal vorticity generated is a function of baroclinity and parcel residence time in the baroclinic zone. Residence time is a function of both storm-relative inflow speed and crossing angle with respect to the baroclinity.

iment (VORTEX; Rasmussen et al. 1994). The third (the Arcadia, OK, supercell of 17 May 1981) has been studied by Dowell and Bluestein (1997).

Analyses were made possible by Mobile Cross-chain Loran Atmospheric Sounding System (M-CLASS) soundings launched during VORTEX field operations, in addition to the high-resolution surface observations of the Oklahoma Mesonet (Brock et al. 1995) and VORTEX mobile mesonet (Straka et al. 1996). In the third case presented [the Arcadia, OK, supercell of 17 May 1981; Dowell and Bluestein (1997)], observations from a 444-m instrumented tower allowed for analysis of cooling rate, depth of cooling, and vorticity generation.

a. 8 June 1995

VORTEX collected data in the vicinity of a broken line of at least a half-dozen supercells. A single, expansive anvil canopy covered most of the eastern Texas panhandle and western Oklahoma in association with the numerous severe storms by 2315 UTC (Fig. 2). South of the anvil shadow, insolation in the cloud-free region allowed for maximum surface temperatures of 33°–34°C, as recorded by southwestern Oklahoma Mesonet stations (Figs. 3 and 4c).[2]

Beneath the thick anvil cirrus shield, the VORTEX mobile mesonet observed temperatures ranging from 26° to 28°C (Fig. 5). Oklahoma Mesonet observations beneath the anvil (Figs. 3 and 4a,b) showed net cooling beginning near 2100 UTC. Incoming shortwave radiation fell from 600–800 W m^{-2} to below 200 W m^{-2} between 2100 and 2200 UTC (Figs. 4a,b). Incoming solar radiation south of the anvil canopy remained above 400 W m^{-2} until after 2300 UTC (Fig. 4c). The difference in shortwave radiation reaching the surface from beneath the anvil canopy to the sunlit ground outside the canopy was approximately 400 W m^{-2} from 2200 to 2300 UTC. However, the anvil also acts to warm the surface via longwave transfer as compared to the cloud-free region, but this difference is only on the order of a few tens of watts per meter squared (Wong et al. 1993; Chin 1994). This differential heating likely played a role in the formation of a temperature gradient that was observed near the edge of the anvil shadow. The location of the strongest surface temperature gradient was not necessarily coincident with the anvil edge (although the southern edge of the temperature gradient should generally be near the edge of the anvil *shadow*, since this is where cooling begins), as the location and movement of the baroclinic zone are a function of both sun angle and the anvil location (Fig. 5).

Outgoing (upwelling) longwave radiation is partially offset by incoming (downwelling) longwave radiation emitted at the blackbody temperature of the anvil. Thus, surface cooling should be most rapid between the time of first shadow (i.e., when the sun is obscured but cirrus is not yet overhead) and the time of overcast. In fact, temperature time series at Chey-

[2] The warm temperatures outside the shadow recorded in southwestern Oklahoma by the mesonet are believed to be accurate since winds were at or above 5 m s^{-1} at all times. Thus, radiational heating effects on the instruments were reduced to within instrument error (±1°C; Richardson 1995; Richardson and Brock 1995).

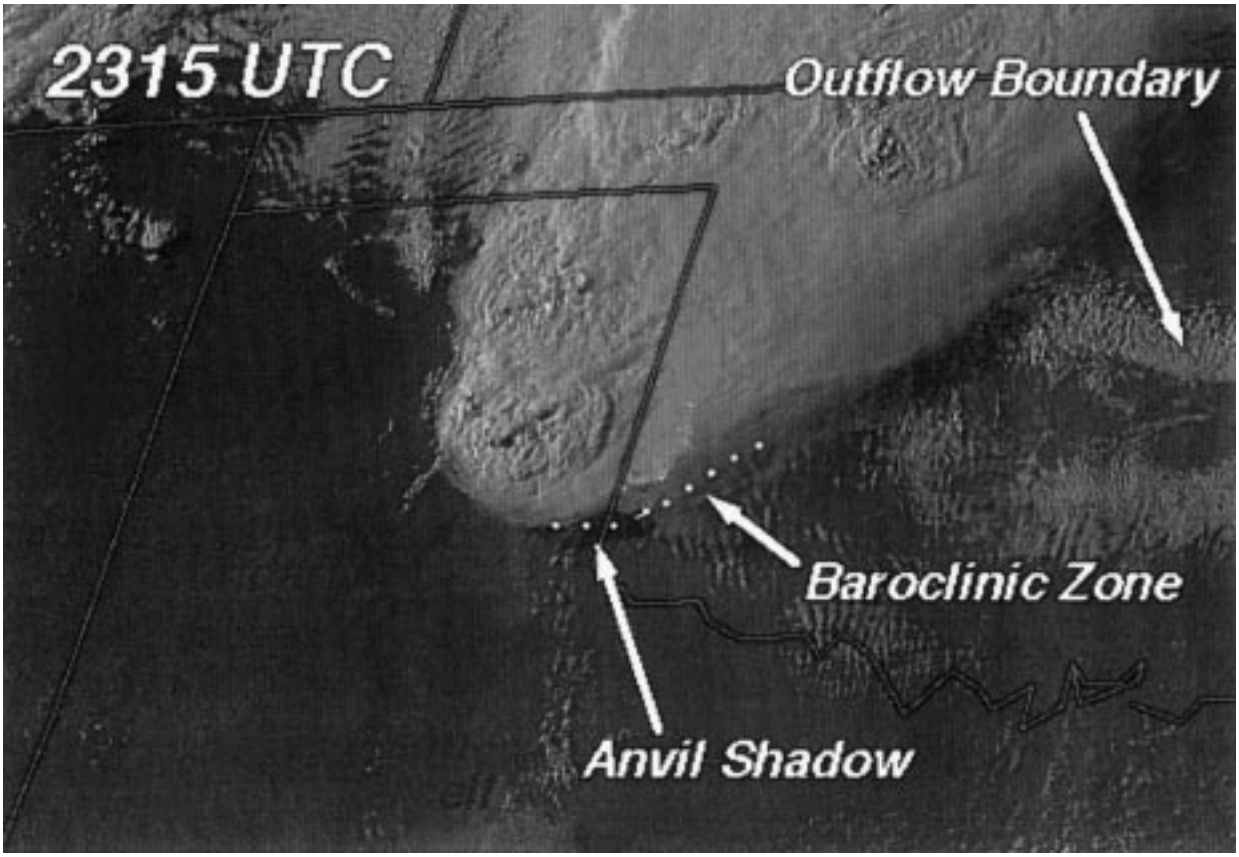

FIG. 2. High-resolution *GOES-8* visible satellite imagery for 2315 UTC 8 June 1995. Strong insolation is reaching the surface south of the anvil edges of the supercell that spawned violent tornadoes near Kellerville and Allison, TX.

enne and Erick (Figs. 4a,b) revealed exactly this behavior. The most rapid cooling lasted approximately 30 min—the time that shading was in progress but cirrus was not yet overhead. A slower cooling rate ensued thereafter (cooling probably also was due to diurnal effects by that time).

The region of surface cooling became collocated with the anvil canopy. A diffuse temperature gradient was present in southwestern Oklahoma prior to the formation of the large anvil canopy (Figs. 3a–c), partially due to terrain ($\sim$1°C of the difference could be explained by elevation differences), and perhaps vegetation or soil moisture differences, but this gradient intensified and became oriented along the anvil shadow edge as the anvil expanded over western Oklahoma.

The temperature gradient present on the southern edge of the anvil weakened by 0100 UTC. The effects of the anvil on shortwave radiation incident at the ground that generated the low-level baroclinity were the same effects that led to the destruction of the baroclinity after sunset. After sunset, cooling was greatest beneath the clear skies south of the anvil, while longwave radiation from the anvil cirrus offset some of the diurnal cooling beneath it (a frontolytic effect).

The buoyancy gradient beneath the anvil edge may have led to significant baroclinic horizontal vorticity generation. The horizontal potential temperature gradient was estimated to be approximately 0.12°C km^{-1} in a zone estimated to be approximately 25 km wide (Table 1). Parcels may have resided in the gradient (yielding $d\eta/dt \sim 3.9 \times 10^{-6}$ s^{-2}; the water vapor mixing ratio gradient was negligible) as long as 2 h, due partly to a small crossing angle (10°) of the storm-relative inflow (11 m s^{-1}) through the temperature gradient (Table 1). (A thorough discussion of storm-relative parcel trajectories and the importance of hodograph structure will follow in the next section.) Neglecting horizontal variations of specific humidity (which were $<$1 g kg^{-1}), the horizontal vorticity generated (augmenting the amount already present due to the large-scale vertical wind shear) may have been as large as 2.7×10^{-2} s^{-1}. We remind the reader that this estimate represents an upper limit; it is a two-dimensional estimate valid for an inviscid atmosphere. The real horizontal vorticity would be different due to friction and tilting/stretching effects. Furthermore, while the exact strength and vertical structure of the baroclinity cannot be assessed without several rawinsondes launched beneath the anvil edge, it is still reasonable to conclude that an important source

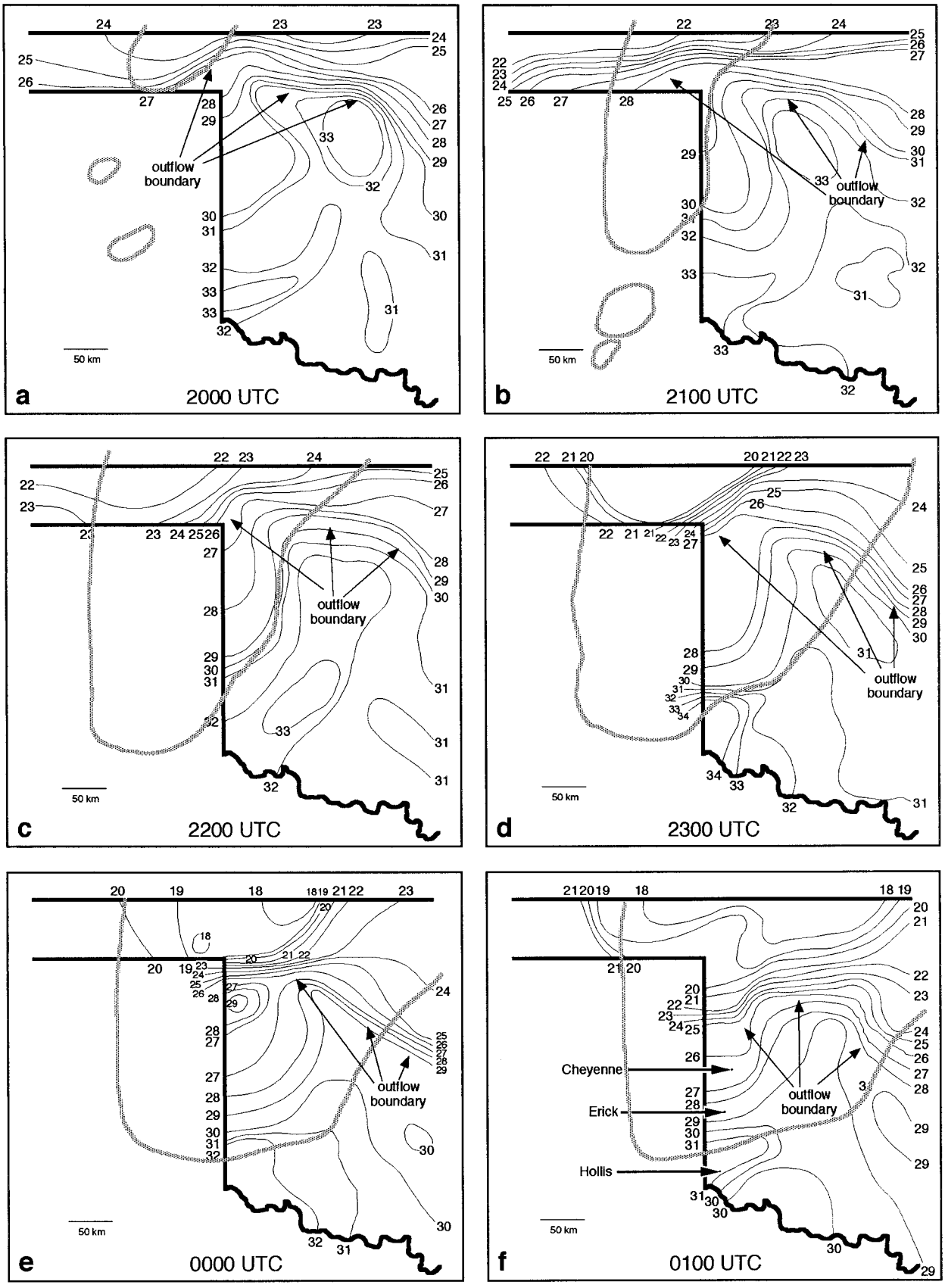
a
2000 UTC
outflow boundary
50 km
b
2100 UTC
outflow boundary
50 km
c
2200 UTC
outflow boundary
50 km
d
2300 UTC
outflow boundary
50 km
e
0000 UTC
outflow boundary
50 km
f
0100 UTC
Cheyenne
Erick
Hollis
outflow boundary
50 km

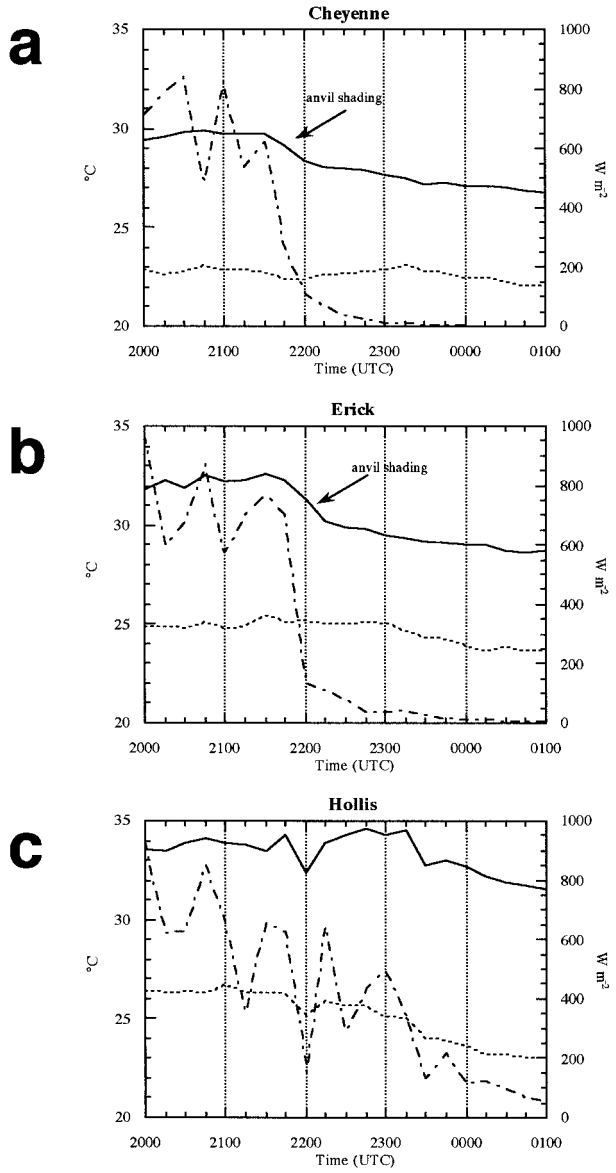

FIG. 4. Time series of temperature (solid) and dewpoint (dashed), both in °C, and incoming solar shortwave radiation (dash–dot trace), in W m^{-2}, from 1900 to 0100 UTC 8–9 June 1995 for (a) Cheyenne, (b) Erick, and (c) Hollis, OK. See Fig. 3f for the locations of these sites.

of near-ground horizontal vorticity (generated over the cooling depth) could be created by an anvil shadow (horizontal vorticity of order 10^{-2} s^{-1}), based on the above calculations and reasonable estimates of the buoyancy gradient and parcel residence times.

Cooling was detected throughout much of the boundary layer (Fig. 6). In the lowest 300 m (935–905 mb), a stable layer was created by the reduction of shortwave radiation (and the associated deficit in the energy budget). Surface temperature had decreased while the mixing ratio had remained constant with time, implying that the cooling in this layer was entirely due to radiative effects. Because of the strong low-level shear and associated mixing, this shallow, slightly stable layer differs from the sharp inversion one might observe at night. In fact, early morning low-level temperature profiles can look very similar despite nocturnal cooling if the vertical wind shear is strong [i.e., low Richardson number; Blackadar (1957); Stull (1988, 504)]. This shallow surface layer was below a shallow, nearly neutral layer that extended from 905 to 870 mb. Above this second layer, up to the level of the capping inversion, was a stabilized and moistened layer.

To summarize, the surface temperature changes could only be associated with radiative effects or advection. Radiative effects are by far the most likely owing to the association with the shadow edge and constant mixing ratio. We reemphasize that our data simply do not permit us to quantify the depth of cooling and, hence, the depth over which the vorticity changes. Nor do we have any direct kinematic evidence of the vorticity changes; only that they are required by the approximated horizontal vorticity equation.

b. 22 May 1995

Convection was initiated during the early afternoon in the eastern Texas panhandle (Fig. 7a). By early evening, a relatively isolated nontornadic supercell[3] was located in the extreme eastern Texas panhandle (Fig. 7b). Data were collected by VORTEX on this storm, and surface observations by the Oklahoma Mesonet detected a region of surface cooling that grew in association with a thick, expanding anvil in western and central Oklahoma.

Similar to the 8 June case, either terrain, vegetation, or soil moisture differences in extreme western Oklahoma may have been responsible for the weak north–south-oriented temperature gradient present prior to anvil shading (Fig. 8a). Following the onset of anvil shading, this gradient intensified since the anvil shadow-edge orientation was near that of the preexisting temperature gradient. The ensuing surface cooling was coincident with the expansion of the anvil shadow (Fig. 8).

[3] Although nontornadic, this storm contained a strong low-level mesocyclone per VORTEX mobile Doppler radar observations.

←

FIG. 3. Oklahoma Mesonet subjectively analyzed surface temperatures at (a) 2000, (b) 2100, (c) 2200, (d) 2300, (e) 0000, and (f) 0100 UTC 8–9 June 1995. Isotherms are drawn at 1°C intervals. The anvil edge is depicted by the thick gray line.

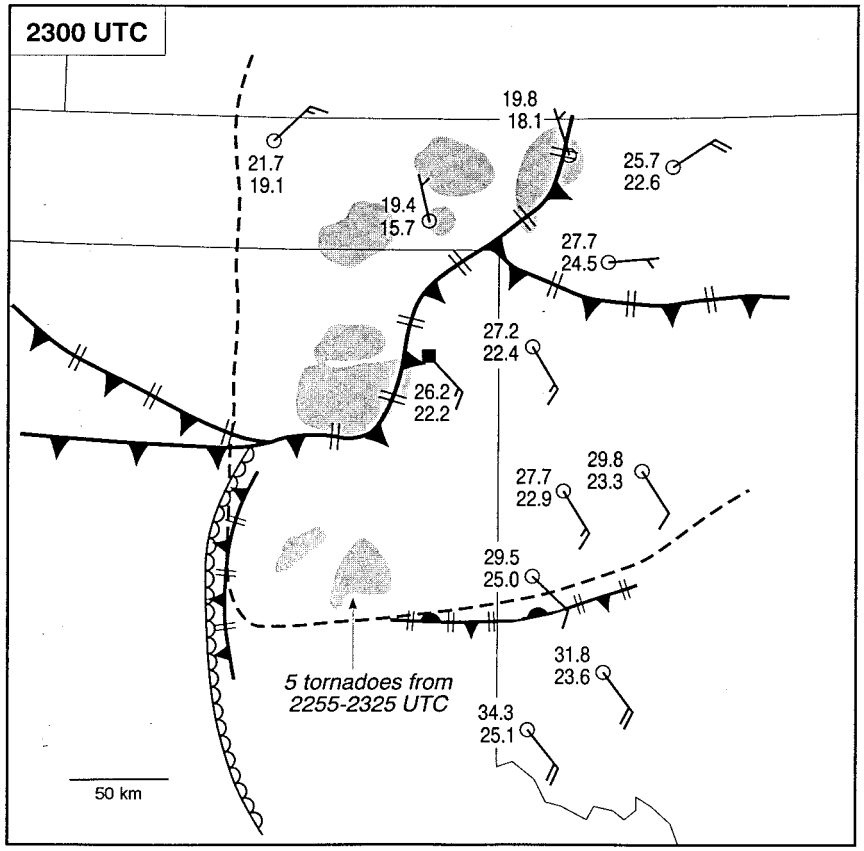

FIG. 5. Mesoscale analysis for 2300 UTC 8 June 1995. Each full wind barb represents 5 m s^{-1}. Temperatures and dewpoints are shown in °C. The open-circled surface observations are from the Oklahoma Mesonet, and the filled square observation is a VORTEX mobile mesonet observation. Radar echoes >35 dBZ are shaded. Fronts are denoted by conventional symbols; however, mesoscale fronts, e.g., outflow boundaries and the anvil-generated baroclinic zone, are depicted using the symbology of Young and Fritsch (1989). The dryline is depicted by the unfilled scalloped line. The anvil canopy edge is depicted by the dashed line.

Surface temperatures beneath the anvil decreased by as much as 3°C in 60 min following the arrival of the cirrus overcast (e.g., Fig. 9a). The surface cooling appeared to be an entirely radiative phenomenon, based on observations of dewpoints remaining constant with time (Fig. 9a). As temperatures fell beneath the anvil in western Oklahoma after 2100 UTC, temperatures in extreme southwestern Oklahoma at sites remaining in sunshine continued to rise in their typical diurnal manner (Figs. 8 and 9b). As observed in the 8 June case, a 400 W m^{-2} difference in incoming shortwave radiation was observed between the shaded region and the clear region from 2145 to 2245 UTC [and similar to the 8 June case, the most rapid cooling occurred between the time of first shadow until conditions were nearly completely overcast (Fig. 9a)]. This differential heating led to a horizontal temperature gradient of approximately 5°C/40 km (Fig. 8b), and a potential temperature gradient of approximately 4°C/40 km.[4] Even more impressive was the skin temperature[5] gradient, obtained from *GOES-8*, which was approximately 10°C/22 km (Fig. 10). (The air temperature gradient was much weaker than the skin temperature gradient, probably reflecting increased surface layer heat fluxes to the south of the baroclinic zone and anvil shadow.)

Given a potential temperature gradient of 4°C/40 km, $d\eta/dt$ was approximately 3.2×10^{-6} s^{-2} (again, the horizontal gradient of specific humidity was small and was neglected). Given the strength of the storm-relative inflow (13 m s^{-1}) and its 45° crossing angle through the baroclinic zone, parcels spent up to 73 min in the

[4] As was the case on 8 June, surface wind speeds were large enough to reduce Oklahoma Mesonet temperature errors to negligible levels.

[5] The skin temperature represents the combined temperature of the topmost layer of soil and vegetation (McNider et al. 1994).

TABLE 1. Observational summary of anvil-generated baroclinity cases.

Case	Estimated baroclinic zone length	Estimated baroclinic zone width	Estimated depth	Amplitude of surface cooling*	Estimated $\lvert\nabla\theta\rvert$	Estimated $d\eta/dt$	Storm-relative inflow crossing angle through baroclinic zone	Estimated maximum parcel residence time	Estimated maximum η generated
8 Jun 1995	100 km	25 km	1000 m	3°C	0.12°C km^{-1}	3.9×10^{-6} s^{-2}	10°	>2 h	2.7×10^{-2} s^{-1}
22 May 1995	110 km	40 km	900 m	3°C	0.10°C km^{-1}	3.2×10^{-6} s^{-2}	45°	73 min	1.4×10^{-2} s^{-1}
17 May 1981	unknown	unknown	>444 m	5°C	unknown	unknown	5°	unknown	9.8×10^{-3} s^{-1}

* For the 8 June and 22 May cases, the amplitude shown is for the first 45 min of cooling, after which it is difficult to remove anvil shading effects from diurnal cooling.

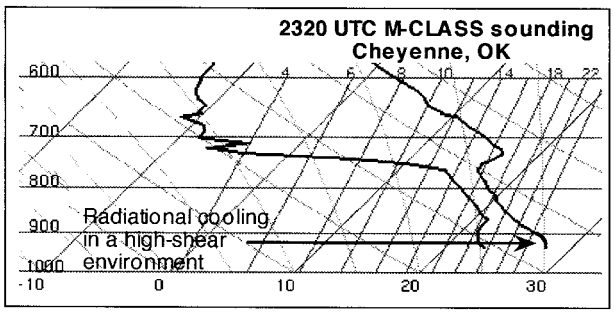

FIG. 6. 2320 UTC 8 June 1995 M-CLASS sounding launched from Cheyenne, OK, beneath a thick anvil. Radiative cooling has occurred in the surface layer, where the formation of an inversion has been precluded by mixing in the presence of strong low-level shear.

40-km-wide zone. This yields a horizontal vorticity increase of $\sim 1.4 \times 10^{-2}$ s^{-1} of the near-ground inflow parcels (Table 1). Once again, this is only an approximation since, in reality, the parcel trajectories are only quasi-horizontal and viscosity and 3D effects alter horizontal vorticity. Moreover, the temperature gradient experienced by parcels along this path is not entirely constant. Nonetheless, it can be said that nontrivial amounts of horizontal vorticity may have been acquired by inflow parcels passing through the anvil-generated baroclinity en route to the storm updraft. Again, more detailed discussion follows in the next section on parcel trajectories and favorable hodograph structure.

Perhaps the most intriguing observations were the boundary layer temperature and moisture profiles revealed by a sounding launched beneath the anvil. The boundary layer lapse rate beneath the anvil was nearly dry adiabatic (8.4°C km^{-1}; Fig. 11) with a constant mixing ratio. Outside of the shadow, the boundary layer probably was also well mixed (Stull 1988). Inspection of the horizontal temperature field, however, clearly revealed the presence of a substantial surface temperature gradient near the southern edge of the anvil (Fig. 8). The well-mixed vertical thermodynamic profile of the boundary layer can be explained by the strong low-level wind shear. But it is the horizontal temperature (buoyancy) gradient that generates horizontal vorticity, not the horizontal variation of lapse rate.

As in the previous case, radiative effects were by far the most likely cause for the formation of the surface temperature gradient, due to the association with the shadow edge and constant mixing ratio. The cooling depth could only be estimated, and hence the exact depth over which the vorticity changes remains unknown.

c. 17 May 1981

A 444-m-tall instrumented tower on the north side of Oklahoma City sampled the low-level environment of a supercell that produced an F2 tornado near Arcadia, Oklahoma, on 17 May 1981 (Dowell and Bluestein 1997). The storm formed shortly before 2100 UTC

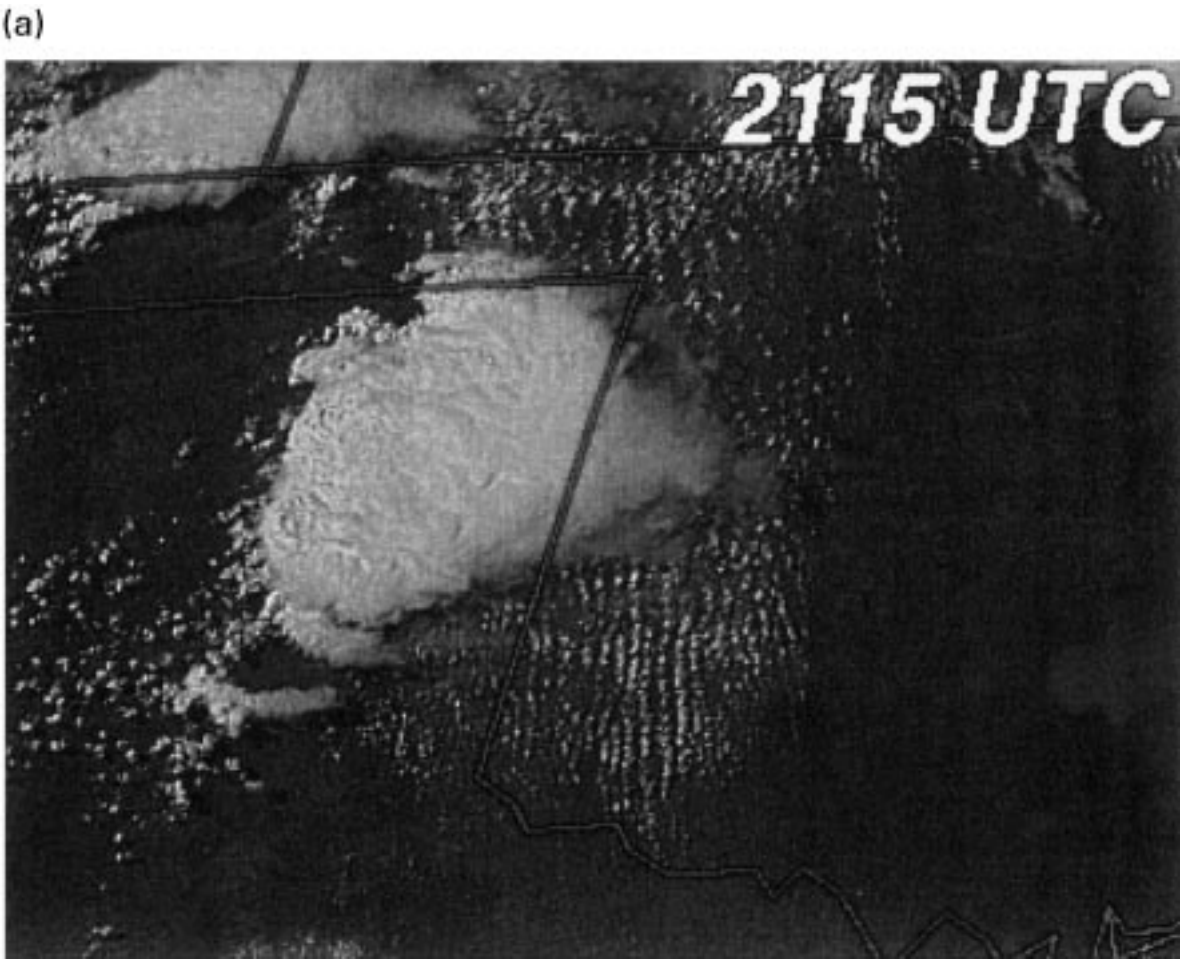

FIG. 7. High-resolution *GOES-8* visible satellite imagery for (a) 2115 and (b) 2315 UTC 22 May 1995. The relatively isolated storm in (b), whose updraft and overshooting top lies in the eastern Texas panhandle, was a nontornadic supercell.

along a dryline approximately 70 km west-southwest of the instrumented tower. As the storm grew, an anvil canopy spread out to the east-northeast (Fig. 12). A cirrus canopy was also associated with a second storm that formed to the south of the Arcadia supercell (Fig. 12); however, a gap between the anvils where shortwave insolation reached the surface was maintained throughout the early evolution of the storms. The low-level updraft and mesocyclone of the Arcadia supercell passed the instrumented tower at 2238 UTC, approximately 20 min before the Arcadia tornado touched down.

The instrumented tower-measured quantities such as wind, temperature, wet-bulb temperature, and incoming shortwave radiation every 1.5 s at as many as seven levels between the surface and 444 m above ground level (AGL) (Dowell and Bluestein 1997). Although the Arcadia storm case lacks the spatial information provided by the Oklahoma Mesonet for the previously discussed storms, a relatively detailed dataset is available at a single location. The observed vorticity changes that will be presented in this case were consistent with anvil-generated baroclinity, but this cannot be definitively demonstrated. Because our analysis was 2D, not 4D, the vorticity budget could not be evaluated.

Vertical shear of the horizontal wind of magnitude 1.0 to 1.5 $\times$ 10^{-2} s^{-1} over the depth of the instrumented tower was characteristic of the sunny environment in Oklahoma City during the late afternoon of 17 May 1981. The hodograph at 2130 UTC (when the Arcadia storm updraft was approximately 50 km west-southwest of the tower and when the anvil shade had just arrived at the tower site) is depicted in Fig. 13. The horizontal vorticity associated with the vertical shear was directed toward the west-southwest. Given the easterly updraft-relative low-level winds (Fig. 13), the horizontal vorticity was considerably streamwise.

Shortly before 2130 UTC, the shortwave radiation received at the tower site (not shown) dropped abruptly from 700 W m^{-2} to less than 140 W m^{-2} (and continued to fall slowly after this initial drop) as the tower entered the shade of the anvil canopy. A gradual cooling of the

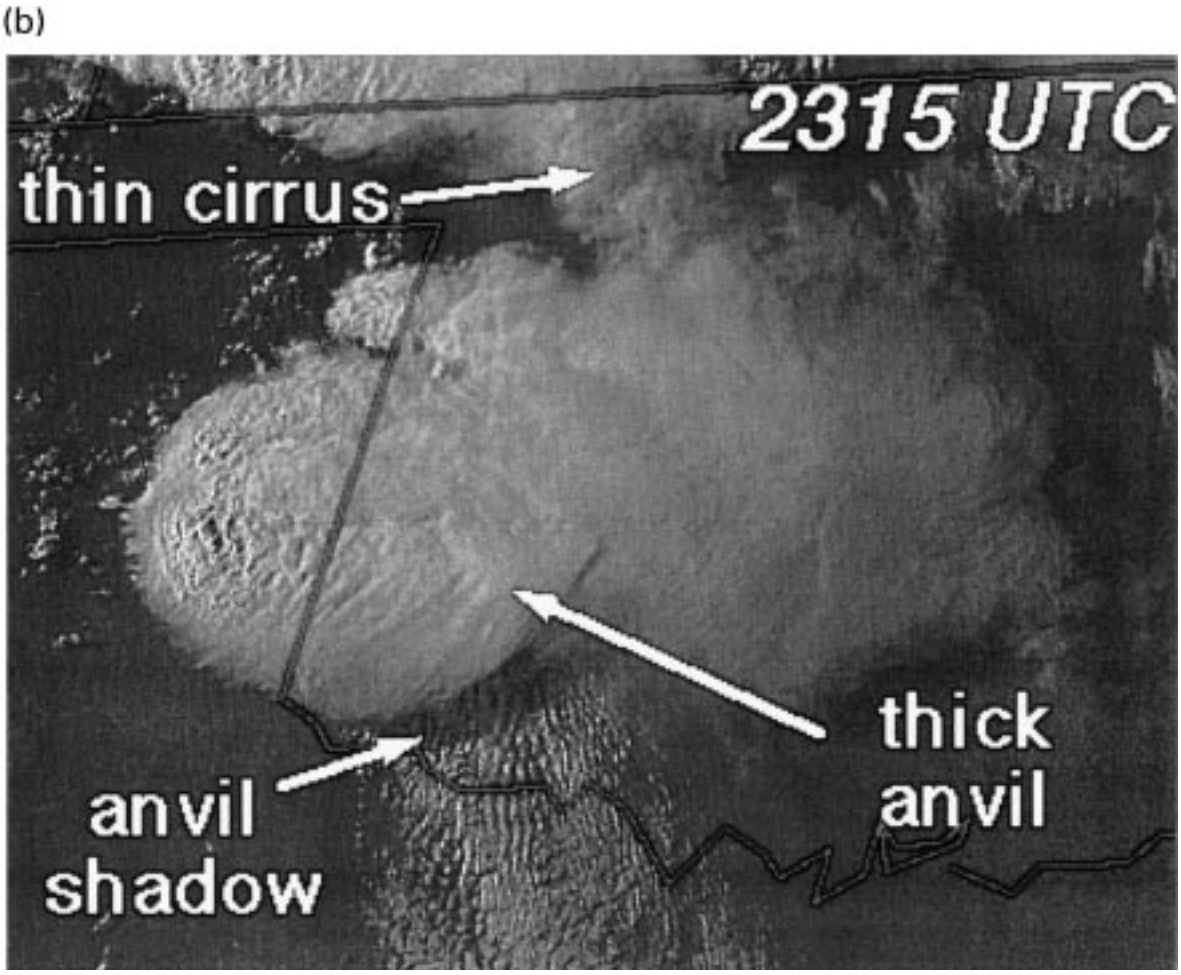

FIG. 7. (*Continued*)

atmospheric boundary layer began at the time of insolation loss (Fig. 14). The cooling was rather steady for a period of over an hour, during which the surface (444 m AGL) temperature dropped 5°C (2°C). The near-surface layer became rather stable (Fig. 15), but the tower measurements between 177 and 444 m AGL indicate a lapse rate remaining close to dry adiabatic. We do not know why the surface layer stabilized in this case and the 8 June case, while in the 22 May case, the entire boundary layer remained nearly dry adiabatic. The vertical wind shear in the lowest 500 m was similar in all three cases ($\sim$0.01 s^{-1}).

Coincident with the boundary layer cooling was a steady increase in the magnitude of the vertical shear of the low-level horizontal winds. By 2234 UTC, when the tower was 2 km east of the updraft, the vertical shear had roughly doubled to 2.8×10^{-2} s^{-1} (Fig. 13). Horizontal stretching was found to have accounted for about 40% of the horizontal vorticity increase (time-to-space conversion was used to estimate the amount of horizontal vorticity stretching). Up to 60%, or about 9.8×10^{-3} s^{-1}, can be attributed to effects other than stretching, including advection, tilting, and baroclinic effects, with anvil-generated baroclinity being one probable candidate.

If vertical motions are ignored, then the horizontal vorticity associated with the vertical shear was directed toward the west-southwest. If a thermally direct vertical circulation existed, then vertical motions may have further contributed to the magnitude of horizontal vorticity along this direction.

Based on the previously discussed cases, we would expect the baroclinic zone in the Arcadia storm inflow at low levels to be oriented along the direction of the anvil edge; that is, isotherms would be oriented from west-southwest to east-northeast (Fig. 12). Horizontal vorticity directed toward the west-southwest would be produced, which is the direction of the observed increase in horizontal vorticity (Fig. 13). The tower observations are thus consistent with a process of horizontal vorticity generation in the baroclinic zone below the southern edge of the Arcadia storm anvil.

It is possible that vorticity generation along a precipitation-induced forward flank rain area may have provided

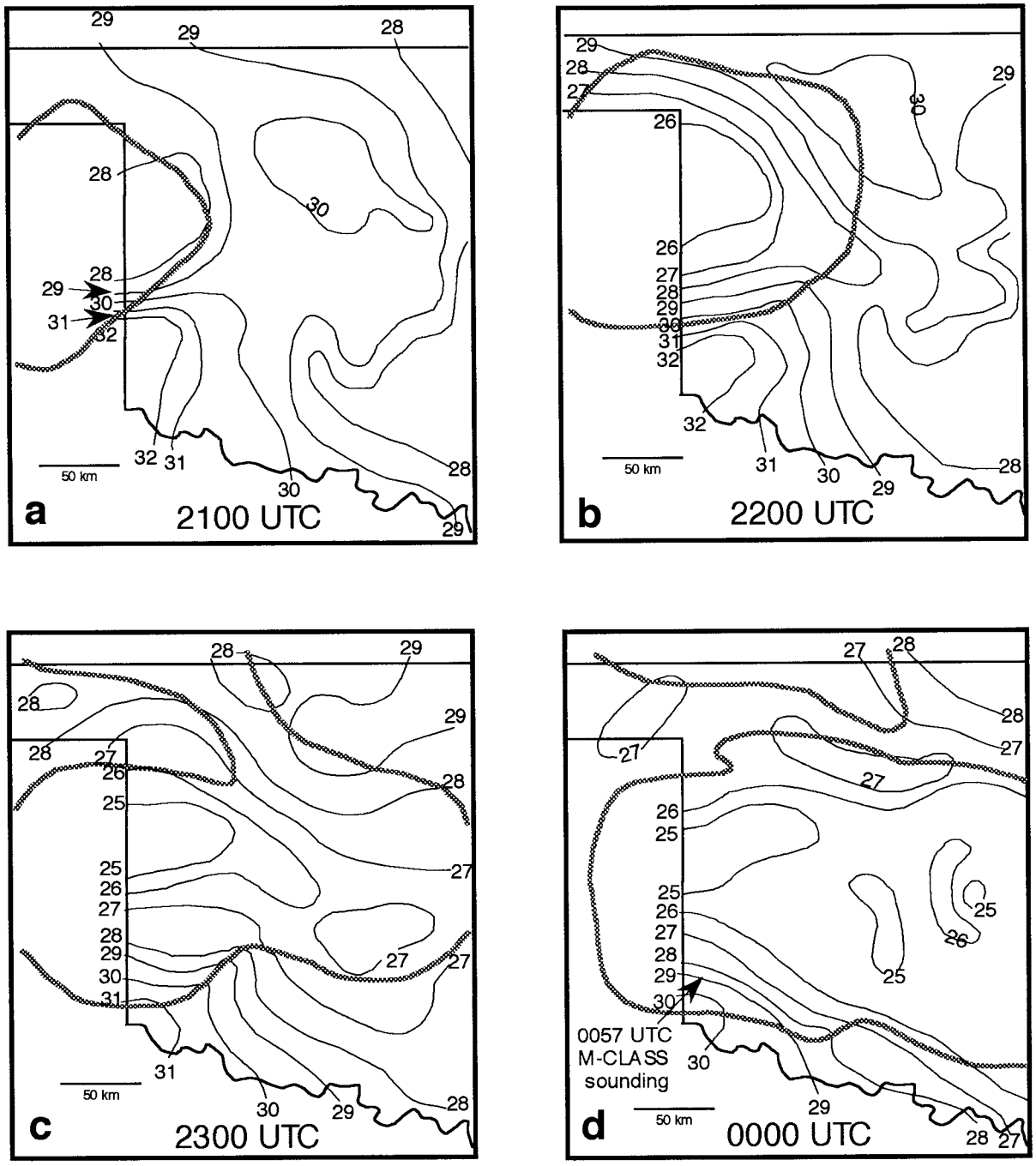

FIG. 8. Oklahoma Mesonet subjectively analyzed surface temperatures at (a) 2100, (b) 2200, (c) 2300, and (d) 0000 UTC 22–23 May 1995. Isotherms are drawn at 1°C intervals. The anvil edge is depicted by the thick gray line. Note the response of the temperature field due to shading by the growing anvil. In (d), the launch site of the M-CLASS sounding shown in Fig. 11 is shown.

a contribution to the vorticity increase; however, we believe it is reasonable that some of the increase was due to anvil shading because of the long period of cooling ahead of the updraft, consistent with cooling on a larger scale than the storm's precipitation region. A forward flank baroclinic zone longer than 50 km would have been present if this were the sole baroclinic cause for the vorticity increase. Additionally, during most of the hour-long cooling period, mixing ratios remained nearly constant, suggesting the cooling was due to radiative causes and not the rain-cooled air mass on the cool side of the forward-flank baroclinic zone.

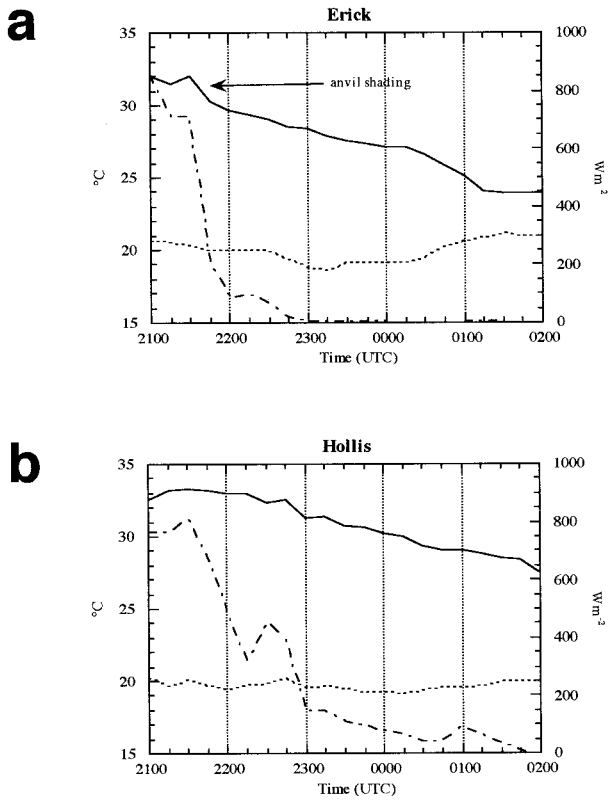

FIG. 9. Time series of temperature (solid) and dewpoint (dashed), both in °C, and incoming solar shortwave radiation (dash–dot trace), in W m^{-2}, from 2100 to 0200 UTC 22–23 May 1995 for (a) Erick and (b) Hollis, OK. See Fig. 3f for the locations of these sites.

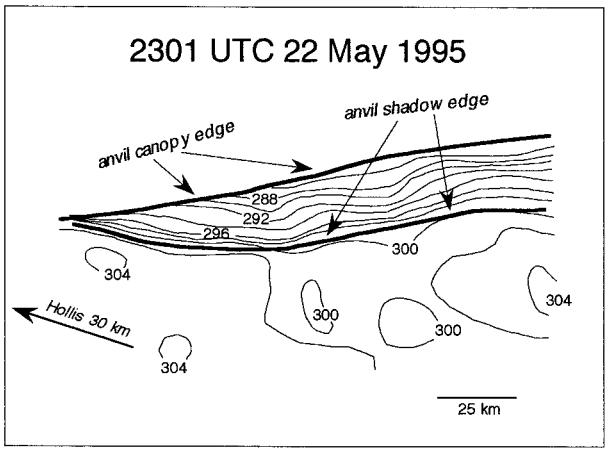

FIG. 10. Skin temperatures at 2301 UTC 22 May 1995 in southwestern Oklahoma near the anvil shadow edge, as determined from *GOES-8*. Isotherms are contoured at 2-K intervals.

3. Importance of hodograph structure

From (1), the amount of horizontal vorticity generated depends as much on the parcel residence time in a baroclinic zone as it does on the strength of the baroclinic zone. For this reason, hodograph shape, or more specifically, storm-relative winds near the ground and near the equilibrium level (where the anvil forms), are critical to generating horizontal vorticity within inflow parcels. Parcels that cross through an anvil-generated baroclinic zone at a large angle (e.g., >45°) will not spend nearly as much time in a baroclinic zone as those that cross at a much smaller angle. This crossing angle is ultimately dictated by hodograph structure. All else being equal, the residence time of parcels in a baroclinic zone is also inversely proportional to the strength of the storm-relative inflow; that is, parcels moving faster through a baroclinic zone will spend less time in the baroclinity (Klemp and Rotunno 1983).

In simplest terms, the anvil edge will generally stream away from an updraft in the direction of the storm-relative wind near the equilibrium level. (This simplification includes only the effects of translation. In reality, there is an additional divergent component to the anvil motion away from its updraft source.) Nearer to the surface, it is the direction of the storm-relative low-level inflow that dictates the trajectories parcels will follow en route to an updraft with respect to the storm.

In the first three cases, the storm-relative inflow in the lowest 500 m (where most of the anvil-generated baroclinity exists) passed through the anvil-generated baroclinity at an angle of 45° or less (Fig. 16). In contrast, in a fourth case in which a well-defined anvil shadow was observed in an otherwise cloud-free region (the VORTEX 6 May 1994 intercept), the storm-relative wind profile was such that near-surface inflow parcels crossed the anvil shadow at nearly a 90° angle, thereby spending only a few minutes in the anvil-generated baroclinity before entering the updraft. For comparison purposes, this hodograph is presented in Fig. 16c.

To maximize the residence time of parcels in baroclinic zones generated by anvils (and to maximize the

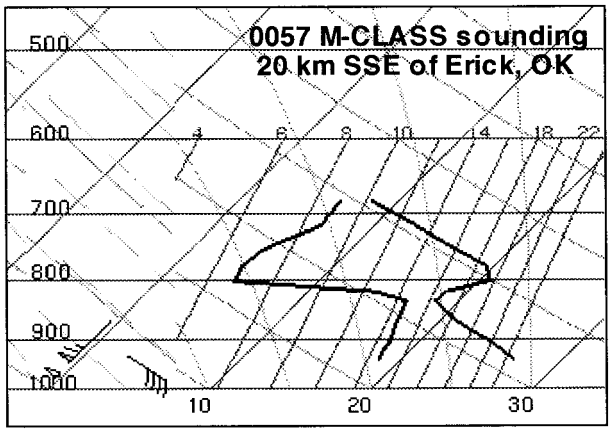

FIG. 11. 0057 UTC 23 May 1995 M-CLASS sounding launched 20 km south-southeast of Erick, OK, beneath the thick anvil shown in Fig. 8. Cooling has occurred, as evidenced by the data shown in Figs. 8 and 9; however, the boundary layer lapse rate has not departed far from a well-mixed state, presumably due to strong boundary layer vertical wind shear.

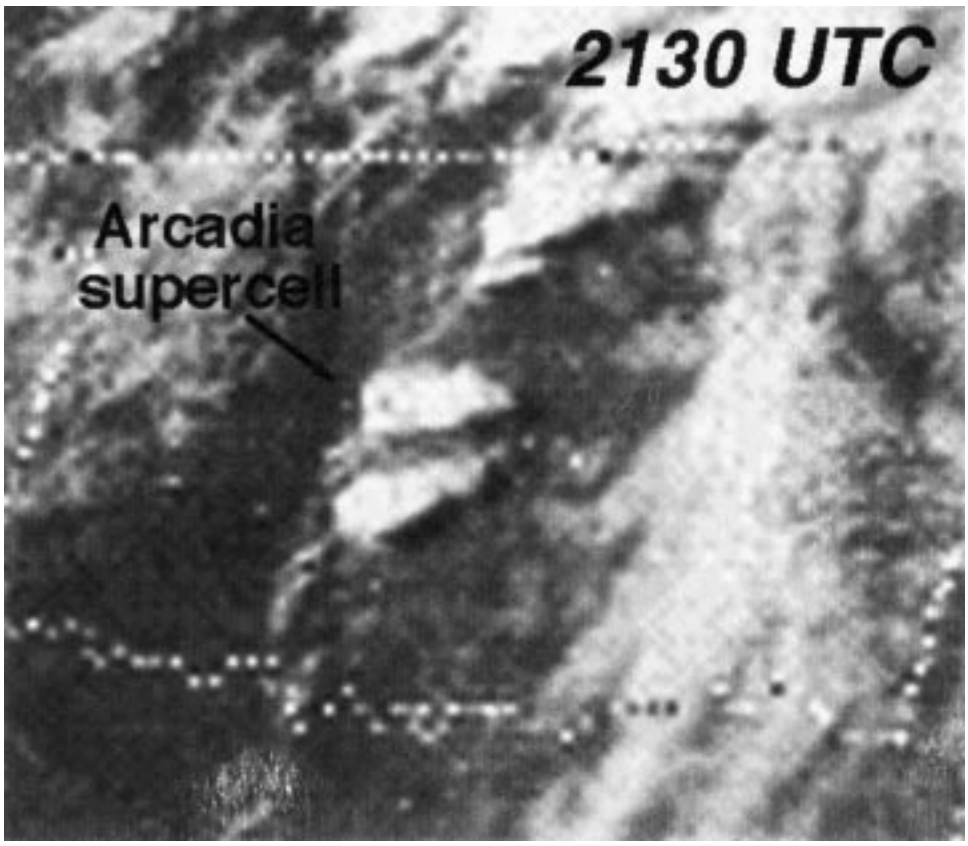

FIG. 12. Visible satellite image at 2130 UTC 17 May 1981.

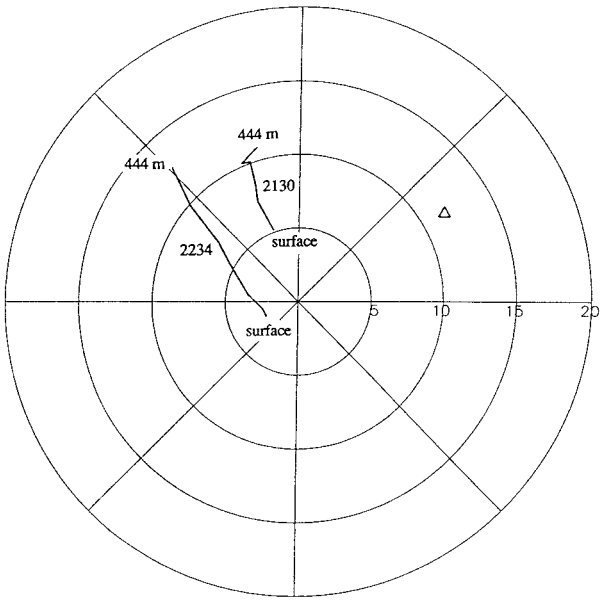

FIG. 13. Hodograph for low-level winds measured by the instrumented tower on the north side of Oklahoma City at 2130 and 2234 UTC 17 May 1981 (adapted from Dowell and Bluestein 1997). Each circle represents 5 m s^{-1} of wind speed. The small triangle indicates observed motion of the Arcadia storm ($u = 10$ m s^{-1}, $v = 6$ m s^{-1}).

horizontal vorticity generated for a given baroclinity magnitude), the storm-relative wind vectors in the near-surface layer (surface to ~500 m) and at the equilibrium level should lie along the same line (either in opposite directions or in the same direction; Figs. 16a,b, 16d, and 17). In other words, the parcel residence time, τ, is

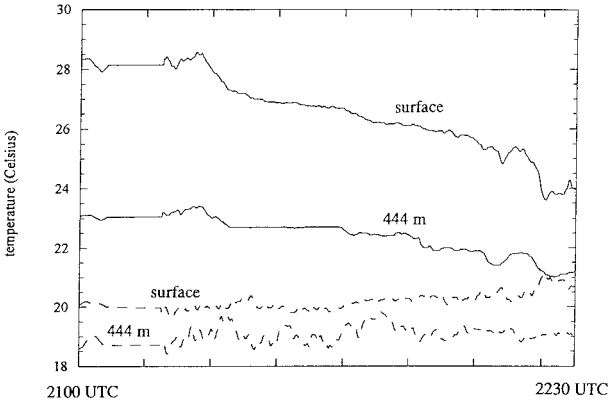

FIG. 14. Time series of temperature (solid, °C) and dewpoint (dashed, °C) measured by the instrumented tower between 2100 and 2230 UTC on 17 May 1981. The heights of the measurements are indicated.

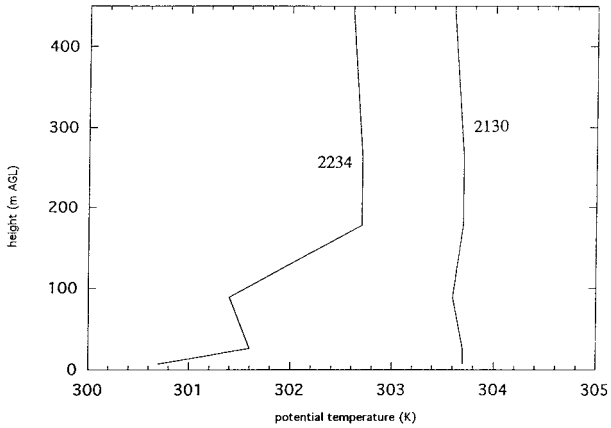

FIG. 15. Vertical profiles of potential temperature at 2130 and 2234 UTC 17 May 1981.

$$\tau \leq \frac{W}{U\cos(90 - \phi)}, \tag{4}$$

where W is the width of the baroclinic zone (normal to the front), U is the storm-relative low-level wind speed, and ϕ is the angle between the virtual isentropes and the storm-relative low-level wind vector in degrees.[6] Since parcels may enter an updraft or exit the boundary layer before crossing the entire baroclinic zone width, (4) is written as an inequality. Of course the baroclinic zone has finite length, L, so an ancillary inequality constraint derives from the advective timescale:

$$\tau \leq \frac{L}{U\cos\phi}. \tag{5}$$

For $\phi = 90°$, the residence time reduces to the advective timescale, thus $\tau \leq W/U$. Similarly, for $\phi = 0°$, $\tau \leq L/U$.

Closer inspection of the hodographs also reveals the following: *to maximize horizontal vorticity generation in the near-ground inflow, the head of the storm motion vector should lie close to the line drawn from the heads of the 0–500-m mean wind vector and the wind vector near the equilibrium level.* This assumes that the baroclinic zone is aligned closely with the anvil edge.

Not only would a small crossing angle between storm-relative inflow and an anvil-generated baroclinic zone ensure longer parcel residence times in the baroclinity, but the horizontal vorticity would have a larger streamwise component. Thus, SRH would be enhanced (Fig. 1). For a 45° parcel crossing angle, the horizontal vorticity would be partitioned equally between the streamwise and crosswise components. For a 90° (0°) parcel crossing angle, the horizontal vorticity generated would be entirely crosswise (streamwise).

4. Implications and concluding remarks

In two of the three cases examined, we found the formation of low-level temperature gradients along the edges of anvil shadows. We believe the temperature gradients owed largely to net radiative cooling in the shadows cast by the optically thick cirrus shields. Residence times in the baroclinity, estimated by analyzing storm-relative winds derived from ''proximity'' hodographs, were shown to potentially allow significant horizontal vorticity ($\sim 10^{-2}$ s^{-1}) to be acquired by updraft inflow parcels. In the third case, vorticity changes consistent with anvil-generated baroclinity were presented.

Supercell anvils tend to be much longer than ordinary storm anvils, since they form in highly sheared environments (Klemp 1987). Long anvils potentially create long baroclinic zones, depending on the opacity of the anvil, thereby allowing inflow parcels more time to acquire horizontal vorticity. When the daytime environment of the storm is relatively cloud free, a favorable scenario for generating baroclinity is established. We believe that the best anvil-generated baroclinic zones occur when clear skies are observed during the entirety of the morning and afternoon, allowing for the maximum possible surface heating outside of the shadows. We extend this hypothesis further by proposing that environments with moderate to high convective inhibition (but not so high as to prevent convection entirely) lacking strong large-scale forcing favor the strongest anvil-generated baroclinity, since isolated storms are more probable in such environments. With little inhibition or strong large-scale forcing, widespread convection would tend to occur, limiting the amount of anvil-induced baroclinity to primarily the southernmost storm (assuming inflow parcels approach from the east or southeast, as is typically observed).

As shown in the previous section, hodograph shape is important for the parcel residence time aspect of the horizontal vorticity generation. But even if a hodograph is known accurately, anticipating whether the storm-relative wind profile will be favorable for significant

[6] In these calculations, we have not considered motion of the baroclinic zones. The motions of the baroclinic zones, as stated in section 2, are a function of the motion of the sun and to the motion of the anvil. Since an anvil has a divergent component to its motion, that is, a component not in the direction of the storm-relative equilibrium level wind (which advects the anvil downstream), an anvil-generated baroclinic zone may move in a direction normal to the equilibrium level storm-relative wind vector. This effect, combined with motion caused by movement of the sun, suggests that we cannot look only at the low-level storm-relative wind and equilibrium level wind vectors to estimate parcel residence times. Incorporating the motion of the baroclinic zone into residence time calculations would be very difficult to do outside of a numerical simulation, since the motion of the sun and the equilibrium level divergence would need to be known (and they likely would not produce steady baroclinic zone motion either). We are granted a reprieve, however. In the 8 June and 22 May cases, the motion of the baroclinic zone was estimated to be 1–3 m s^{-1}. Since this is much less than the storm-relative low-level inflow (>10 m s^{-1}), we neglected the motion of the baroclinic zone. We do not know whether this assumption would be valid in all cases. In the 17 May 1981 case, the motion of the anvil-generated baroclinic zone could not be determined.

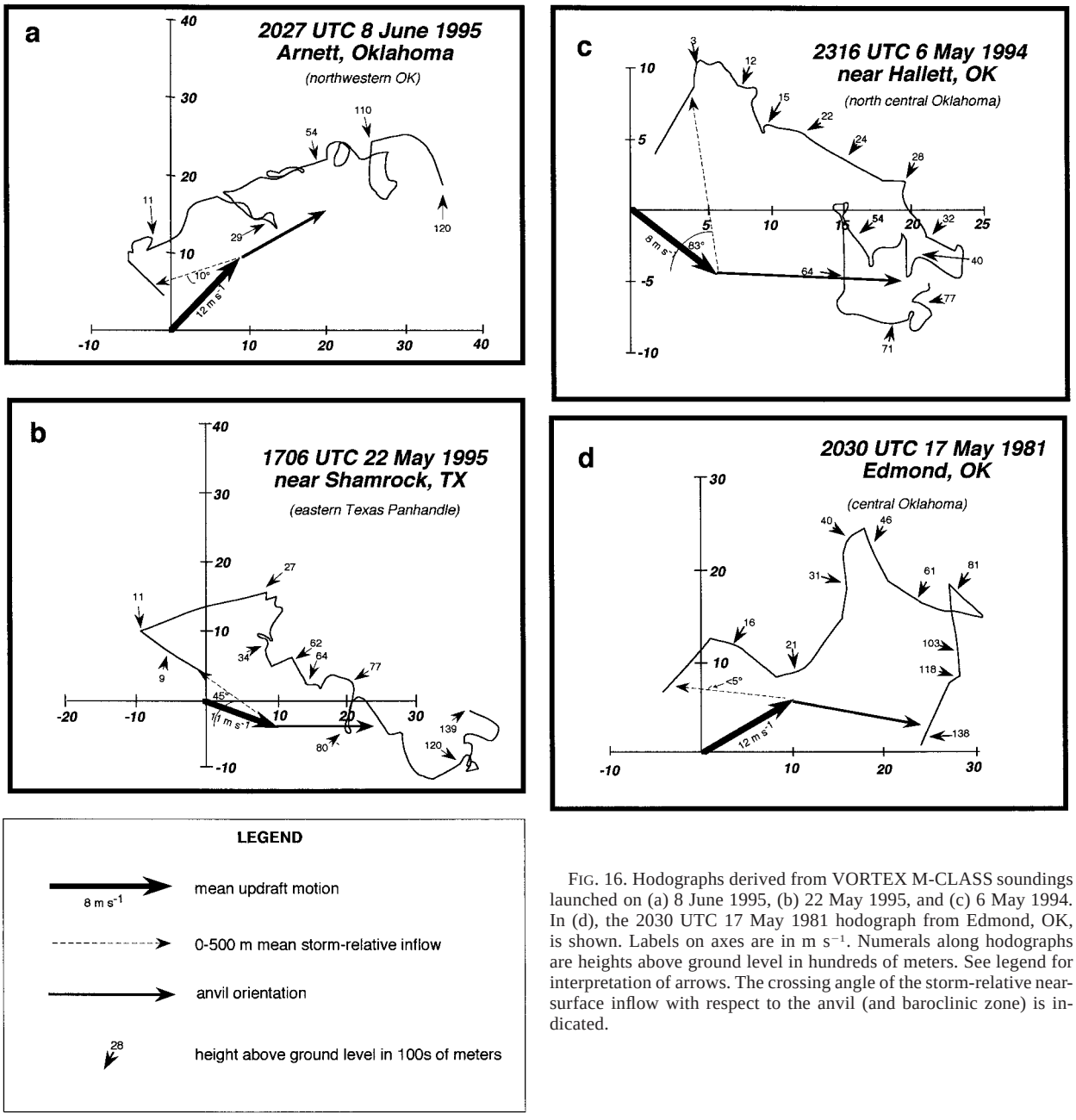

FIG. 16. Hodographs derived from VORTEX M-CLASS soundings launched on (a) 8 June 1995, (b) 22 May 1995, and (c) 6 May 1994. In (d), the 2030 UTC 17 May 1981 hodograph from Edmond, OK, is shown. Labels on axes are in m s^{-1}. Numerals along hodographs are heights above ground level in hundreds of meters. See legend for interpretation of arrows. The crossing angle of the storm-relative near-surface inflow with respect to the anvil (and baroclinic zone) is indicated.

horizontal vorticity generation, given that substantial baroclinity can be generated by an anvil, would be a difficult task due to the uncertainty in forecasting storm motions. Storm-relative inflow speeds are also a parcel residence time determinant.

These observations may highlight a shortcoming of numerical models that fail to simulate temperature contrasts associated with differential heating near an anvil edge. When a 5°–7°C temperature gradient (Fig. 3d) is not captured in a supercell numerical simulation, an important forcing possibly is being missed.

The most difficult problem may be to assess the importance of the depth over which the horizontal vorticity is generated. Certainly if the baroclinic vorticity generation zone is very shallow (<250 m), then SRH would probably be enhanced only slightly, since SRH is typically an integral over a 2–3-km depth (e.g., Davies-Jones 1984; Fig. 1). However, the precise depth over which inflow horizontal vorticity is important for the generation of strong vertical vorticity following tilting and stretching is a question that remains to be answered, in addition to the question of the importance of the

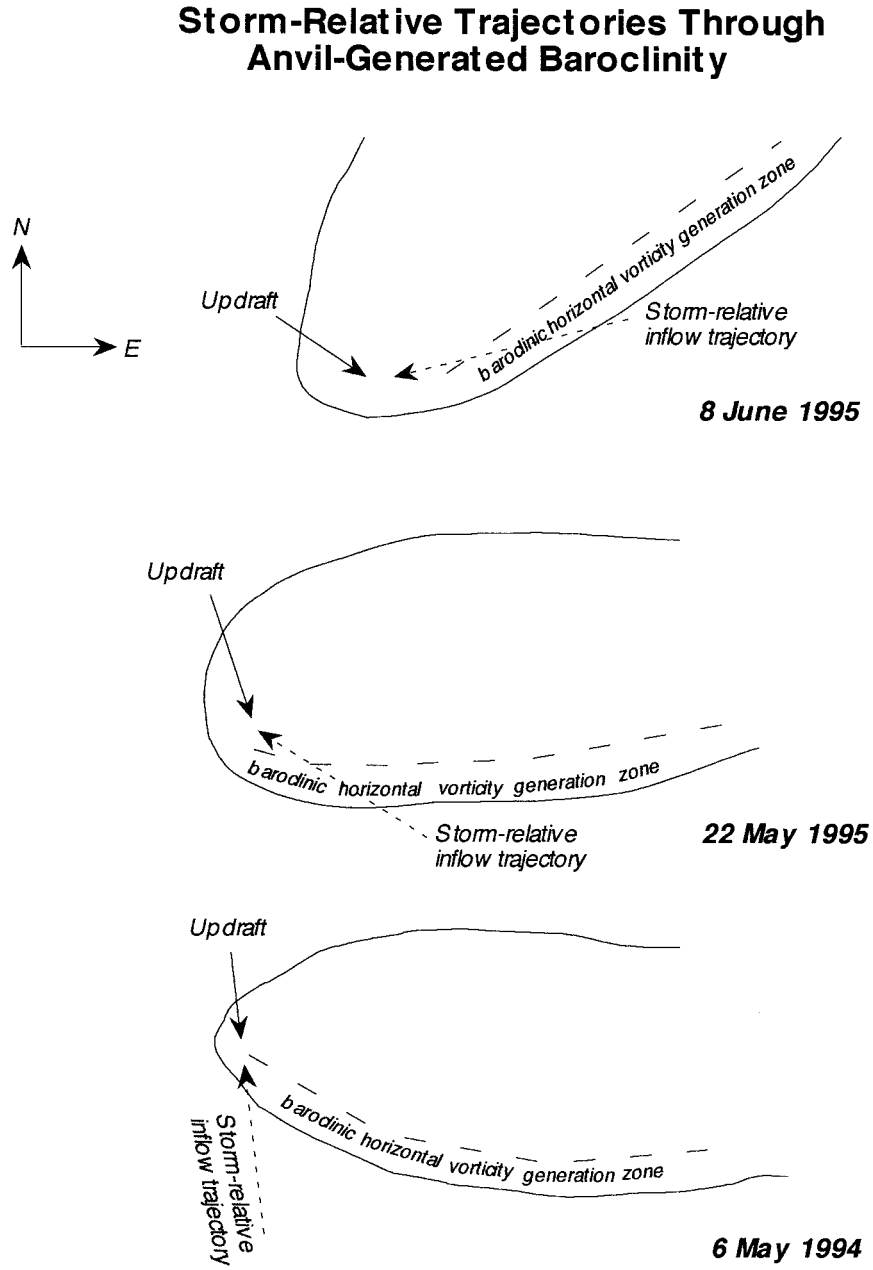

FIG. 17. Schematic representation of the storm-relative trajectories through the anvil-generated baroclinic zones on 8 June 1995, 22 May 1995, and 6 May 1994. In the first two cases, not only does the vorticity generated contain a greater streamwise component, but the parcel residence times in the baroclinity are longer. See Figs. 16a,b for examples of hodographs that would favor the first two scenarios for extended baroclinic vorticity generation, and Fig. 16c for an example of a hodograph that would not provide a favorable storm-relative flow for long parcel residence times in anvil-generated baroclinity.

orientation of the horizontal vorticity (e.g., streamwise versus crosswise).

Although diffuse, the baroclinic zones produced by anvil-induced differential heating presented in this manuscript were as well defined as the forward-flank baroclinic zones along the edges of precipitation cores sampled on several VORTEX days (e.g., 2 June 1995, 8 June 1995, 16 May 1995). Rotunno and Klemp (1985) hypothesized that the forward-flank baroclinic zone ultimately provided the source of low-level vertical vorticity in supercells. If the low-level (e.g., 1–3 km AGL) mesocyclone is proven to be formed from the tilting and stretching of vortex lines that mainly originate in a baroclinic layer, then a radiationally forced baroclinic effect

may be important for the vorticity dynamics of the low-level mesocyclone. [The horizontal vorticity capable of being generated by the baroclinic zones presented in this study is of similar magnitude to the horizontal vorticity generated in the precipitation-induced forward-flank baroclinic zones studied by Klemp and Rotunno (1983) and observed during other VORTEX cases yet to be formally published. In the anvil-generated baroclinity cases, the vorticity generation rates were smaller but residence times were longer. In the precipitation-induced forward-flank cases, the generation rates were larger (due to stronger baroclinity), but residence times were shorter.]

A small field experiment may be conducted in the spring of 1998 to better sample the vertical structure of these baroclinic zones. More quantified horizontal vorticity estimates are needed to assess the significance of the horizontal vorticity augmentation due to the baroclinic zones. Future work will also include attempts to create anvil-generated baroclinic zones in numerical simulations. An interesting question to address is whether it is possible for mesocyclogenesis to occur in a storm that ingests parcels whose *only* horizontal vorticity source is baroclinic generation along an anvil-generated boundary.

Acknowledgments. We are indebted to careful reviews by Drs. Conrad Ziegler and Bob Maddox, as well as constructive discussions with Drs. Scott Richardson and Todd Crawford. The manuscript also was improved by the insightful comments of three anonymous reviewers. Joan O'Bannon and Sue Weygandt drafted several figures. We are also grateful to all VORTEX volunteers, Dr. David Blanchard, Dr. John Weaver, Mark Shafer, Daphne Zaras, and Tom Condo. Some data were obtained from the Atmospheric Radiation Measurement program sponsored by the U.S. Department of Energy, Office of Energy Research, Office of Health and Environmental Research, Environmental Sciences Division. A portion of this work was funded by NSF Grants ATM-9302379, ATM-9617318, and EAR-9512145. In addition, support was provided by a grant from the NSF Science and Technologies Center, Center for the Analysis and Prediction of Storms (ATM-9120009). The lead author was supported by an AMS fellowship provided by GTE Federal Systems Division, Chantilly, Virginia.

REFERENCES

Blackadar, A. K., 1957: Boundary layer wind maxima and their significance for the growth of nocturnal inversions. *Bull. Amer. Meteor. Soc.*, **38,** 283–290.

Brock, F. V., K. Crawford, R. Elliot, G. Cuperus, S. Stadler, H. Johnson, and M. Eilts, 1995: The Oklahoma Mesonet: A technical overview. *J. Atmos. Oceanic Technol.*, **12,** 5–19.

Chin, H.-N. S., 1994: The impact of the ice phase and radiation on a midlatitude squall line system. *J. Atmos. Sci.*, **51,** 3320–3343.

Davies-Jones, R. P., 1984: Streamwise vorticity: The origin of updraft rotation in supercell storms. *J. Atmos. Sci.*, **41,** 2991–3006.

Dowell, D. C., and H. B. Bluestein, 1997: The Arcadia, Oklahoma, storm of 17 May 1981: Analysis of a supercell during tornadogenesis. *Mon. Wea. Rev.*, **125,** 2562–2582.

Gray, W. M., and R. W. Jacobson Jr., 1977: Diurnal variation of deep cumulus convection. *Mon. Wea. Rev.*, **105,** 1171–1188.

Klemp, J. B., 1987: Dynamics of tornadic thunderstorms. *Annu. Rev. Fluid Mech.*, **19,** 369–402.

——, and R. Rotunno, 1983: A study of the tornadic region within a supercell thunderstorm. *J. Atmos. Sci.*, **40,** 359–377.

Lilly, D. K., 1986: The structure, energetics, and propagation of rotating convective storms. Part II: Helicity and storm stabilization. *J. Atmos. Sci.*, **43,** 126–140.

McNider, R. T., A. J. Song, D. M. Casey, P. J. Wetzel, W. L. Crosson, and R. M. Rabin, 1994: Toward a dynamic–thermodynamic assimilation of satellite surface temperature data in numerical atmospheric models. *Mon. Wea. Rev.*, **122,** 2784–2803.

Rasmussen, E. N., J. M. Straka, R. P. Davies-Jones, C. A. Doswell III, F. H. Carr, M. D. Eilts, and D. R. MacGorman, 1994: Verification of the Origins of Rotation in Tornadoes Experiment: VORTEX. *Bull. Amer. Meteor. Soc.*, **75,** 995–1006.

Richardson, S. J., 1995: Passive solar radiation shields: Numerical simulation of flow dynamics. Preprints, *Ninth Symp. on Meteorological Observations and Instrumentation,* Charlotte, NC, Amer. Meteor. Soc., 253–258.

——, and F. V. Brock, 1995: Passive solar radiation shields: Energy budget—Optimizing shield design. Preprints, *Ninth Symp. on Meteorological Observations and Instrumentation,* Charlotte, NC, Amer. Meteor. Soc., 259–264.

Rotunno, R., and J. B. Klemp, 1985: On the rotation and propagation of simulated supercell thunderstorms. *J. Atmos. Sci.,* **42,** 271–292.

——, ——, and M. L. Weisman, 1988: A theory for strong, long-lived squall lines. *J. Atmos. Sci.,* **45,** 463–485.

Segal, M., J. F. W. Purdom, J. L. Song, R. A. Pielke, and Y. Mahrer, 1986: Evaluation of cloud shading effects on the generation and modification of mesoscale circulations. *Mon. Wea. Rev.,* **114,** 1201–1212.

Straka, J. M., E. N. Rasmussen, and S. E. Frederickson, 1996: A mobile mesonet for fine-scale meteorological observations. *J. Atmos. Oceanic Technol.,* **13,** 921–936.

Stull, R. B., 1988: *An Introduction to Boundary Layer Meteorology.* Kluwer Academic, 666 pp.

Wong, T., G. L. Stephens, P. W. Stackhouse Jr., and F. P. J. Valero, 1993: The radiation budgets of a tropical mesoscale convective system during the EMEX-STEP-AMEX experiment, 2. Model results. *J. Geophys. Res.,* **98,** 8695–8711.

Young, G. S., and J. M. Fritsch, 1989: A proposal for general conventions in analysis of mesoscale boundaries. *Bull. Amer. Meteor. Soc.,* **70,** 1412–1421.